Project: 1190
Project title: JPI Oceans / JPI Climate project ROADMAP
Principal investigator: Dr. Daniela Matei
Allocation period: 2021-01-01 to 2021-12-31

Achievements in 2021

Partially coupled experiments with MPI-ESM

Short-term air-sea interactions and the role of ocean and atmosphere initial conditions for the atmospheric response to Arctic sea ice loss are explored, following the protocol designed by the PAMIP (Polar Amplification Model Intercomparison Project, Smith et al. 2019) on partially coupled experiments. Here we report first results of the partially coupled experiments performed with the MPI-ESM model. We use the Max Planck Institute for Meteorology Earth System Model (MPI-ESM1.2, Mauritsen et al. 2019), applying a T127 spectral grid (about 1^o resolution) and 95 hybrid levels in the atmosphere (top at 80 km), and a tripolar grid (two northern poles) with a 0.4^o nominal resolution and 40 unevenly spaced depth levels in the ocean. Altogether, we have performed 720 ensemble members (with an integration length of 14 months each), 240 members respectively prescribing the PAMIP *piArctic*, *present-day* and *fut2CArctic* sea ice extent.

The PAMIP sea ice extent (target) is interpolated bilinearly to the oceanic model grid and linearly to daily resolution. In the model simulations, the sea ice extent is constrained at every ocean time step by Newtonian relaxation ("nudging") towards the target with a damping factor of one day. The same approach is used in house to initialize the sea ice extent in prediction experiments (Bunzel et al. 2016). The simulated sea ice extent in all ensemble members closely follows the PAMIP sea ice extent (Figure 1).

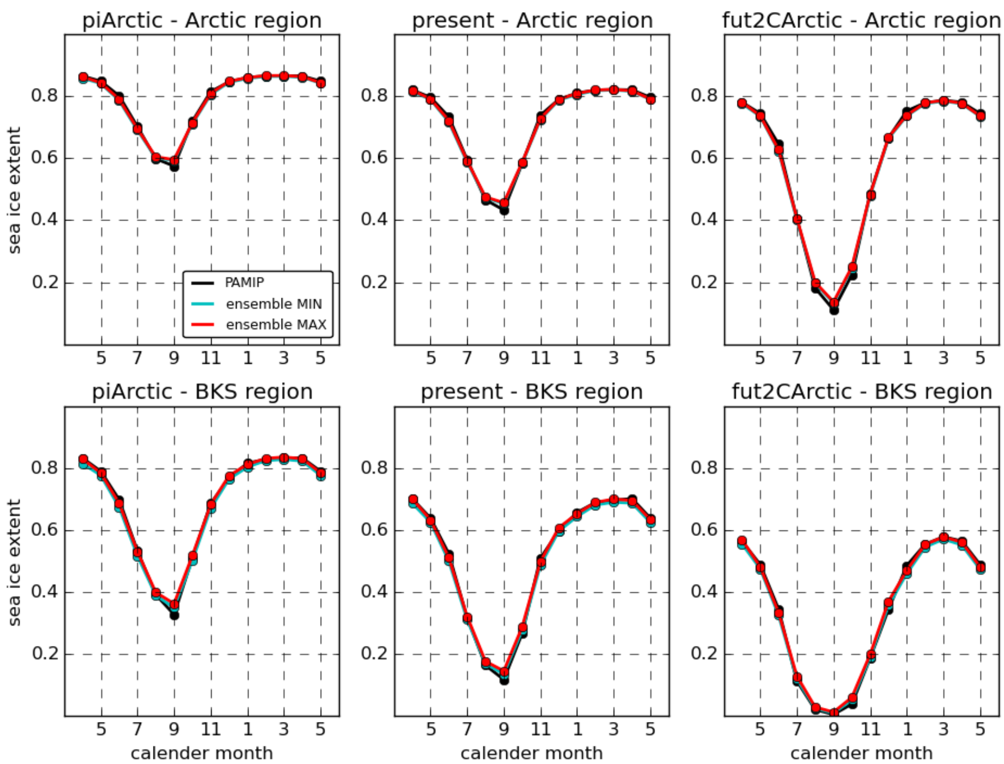

Figure 1: Time series of the sea ice extent [0-1] averaged over the Arctic (poleward of 67.5^{o}N) and the Barents-Kara-Sea (25^{o}E-100^{o}E, 65^{o}N-82.5^{o}N) in the experiments prescribing the piArctic, present and fut2CArctic PAMIP

sea ice extent. The cyan and red line respectively correspond to the ensemble minimum and maximum. The PAMIP sea ice extent (interpolated to the model grid prior to area-averaging) is shown in black.

Initial conditions are taken from ten historical CMIP6 simulations (period 1985-2014) performed with MPI-ESM1.2. We have combined 30 oceanic initial states with eight atmospheric initial states, yielding the required 240 initial conditions. Regarding the oceanic initial states, 15 correspond to an AMV+IPV- state and 15 to an AMV-IPV+ state. These states are chosen based on the strength of the AMV and IPV index as well as on the SST anomaly pattern for the individual years. The AMV+IPV- and AMV-IPV+ ocean states have been computed and selected following the Blue Action WP3 Coordinated Experiment Protocol, and considering the whole historical experiment for the identification of the AMV and IPV indices. Regarding the atmospheric initial states, 4 correspond to an easterly QBO phase and 4 to a westerly QBO phase. The easterly / westerly QBO phases have been selected by finding the years where the November zonal mean zonal winds at 50 hPa, averaged over 5^{o}S-5^{o}N, are < -5 m/s (EQBO) or > +5 m/s (WQBO). CMIP6 external radiative forcing corresponding to year 2000 is applied. In the following, all analyses are reported for DJF averages.

DJF circulation response

Figure 2 shows the DJF (December to February) near surface semperature for the AMV-IPV+ minus AMV+IPV- difference of the *present-day* ensemble means. The typical anomaly patterns of IPV+ minus IPV- over the Pacific and of AMV- minus AMV+ over the Atlantic oceans emerge, confirming the success of the design of the experiments.

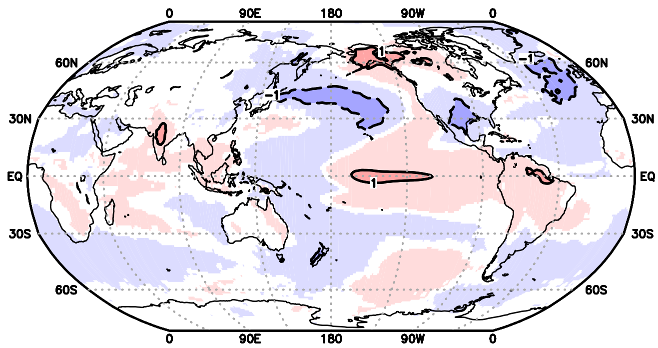

Figure 2: DJF (December to February) near surface temperature (K) for the AMV-IPV+ minus AMV+IPV- difference of the *present-day* ensemble means. Shading indicates significance at $p < 0.05$.

Although the initialization of the QBO is successful, the impact of the QBO phase on the NH stratosphere vortex is severely underestimated, possibly because the QBO signal is relatively small and/or the weak vortex bias of the model (Figure 3). No QBO impact on the atmospheric dynamical response to sea ice loss is indeed found. Therefore, in the following we are not stratifying by the phase of the QBO.

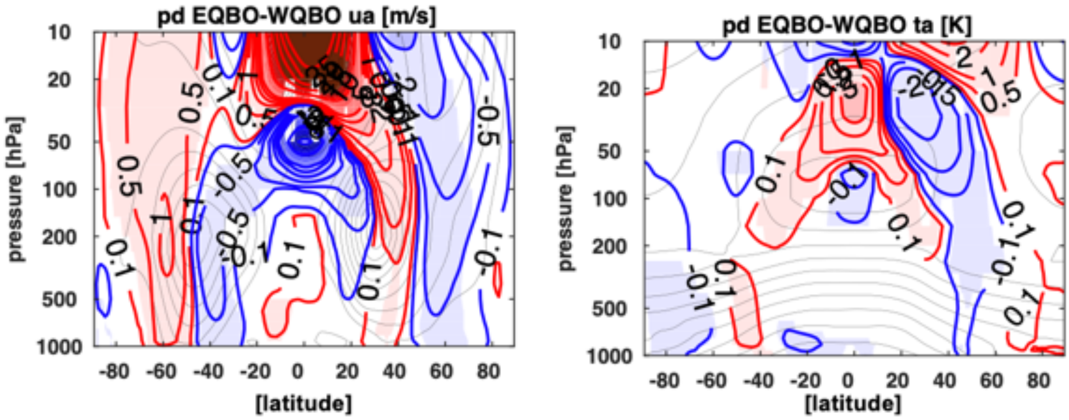

Figure 3 DJF (December to February) zonal mean zonal wind (m/s) for the EQBO minus WQBO difference of the present-day ensemble means. Shading indicates significance at $p < 0.05$.

By including short-term air-sea interactions, the global response to sea ice loss is found sensitive to the Arctic sea ice extent. The sensitivity to Arctic sea ice extent is evaluated by comparing the response to the change from either the *present-day* or *piArctic* (preindustrial) to the *fut2CArctic* (future) Arctic sea ice extent. A substantial zonal mean zonal wind response, the equatorward shift in the midlatitude westerlies, is reported for the preindustrial to the future Arctic sea ice loss (Figure 4, right). The substantial zonal mean zonal wind response is accompanied by a large-scale mid-latitude and tropical atmospheric cooling (Figure 4, left), suggesting a role for air-sea interaction in the amplification of the signal. In general, the stratosphere does not seem to play a (significant) role in the responses.

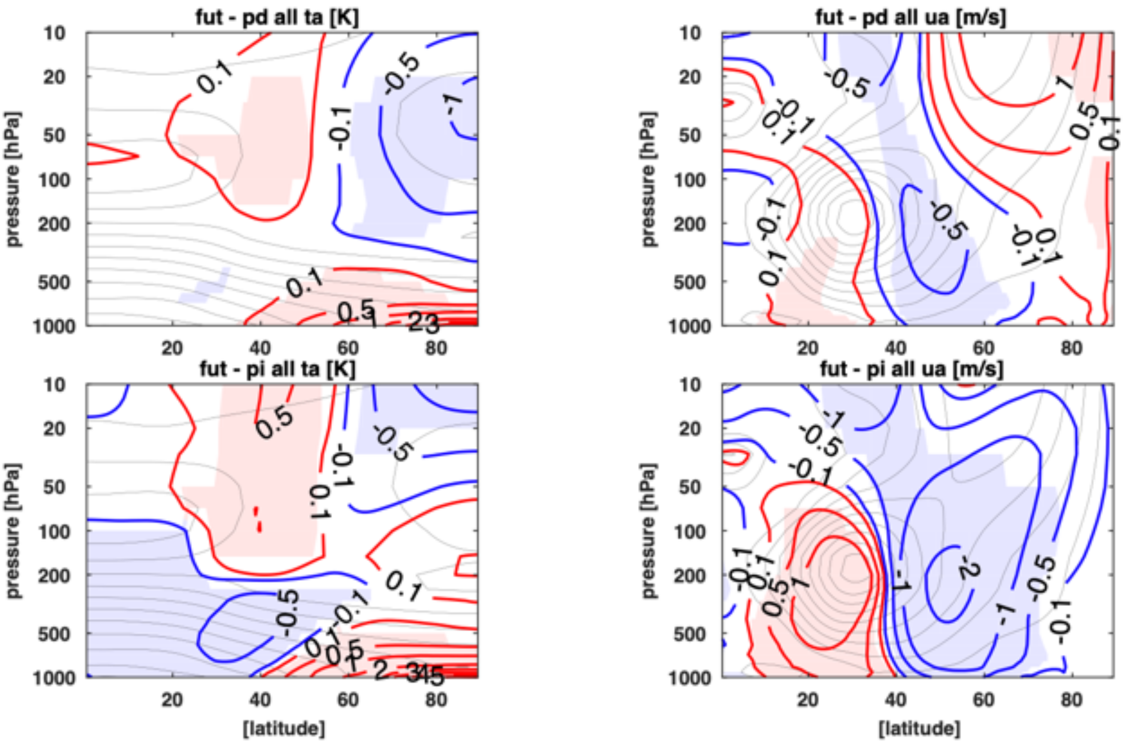

Figure 4: DJF (December to February) difference of the *fut2CArcti* minus *present-day* (upper rows) and *fut2CArcti* minus *piArctic* (lower rows) ensemble means, zonal mean temperature (K) (at left) and zonal mean

zonal wind (m/s) (at right). Shading indicates significance at $p < 0.05$. Gray contours show *present-day* (upper rows) / *piArcti* (lower rows) respective ensemble mean.

Sensitivity to the ocean initial conditions is investigated by comparing the responses to Arctic sea ice loss for the ensemble means with AMV+IPV- and AMV-IPV+ ocean initial states. We find that the ocean initial conditions appear to have little influence on the global response to sea-ice loss. Instead, they affect the response over central Siberia (Figure 5). The minus AMV-IPV+ minus AMV+IPV- difference shows a clear high pressure localized anomaly over Siberia, accompanied by a distinct cooling, suggesting that a mid-latitude continental cooling in response to Arctic sea ice loss can be mediated by the ocean state. This response is slightly more evident for the *fut2CArcti* minus *present-day* than *fut2CArcti* minus *piArctic.* Further changes in the responses are seen around the North Pacific rim and Western Europe.

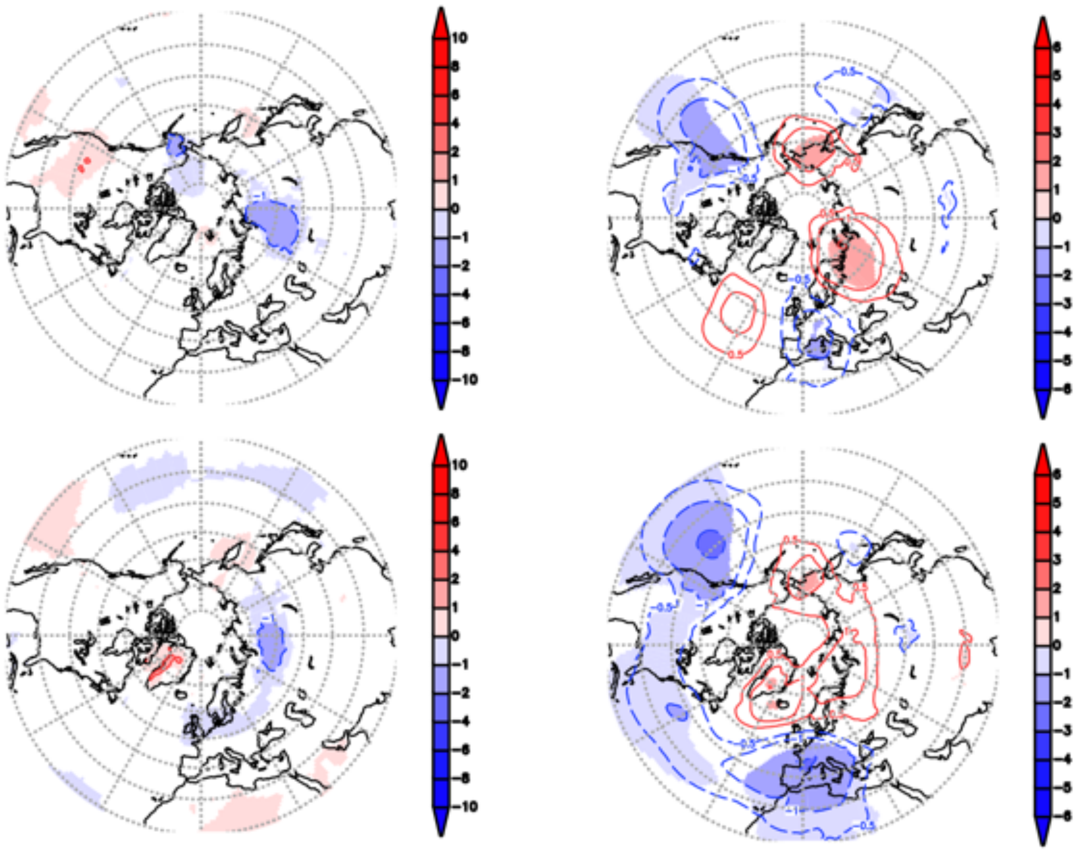

Figure 5: DJF (December to February) AMV-IPV+ minus AMV+IPV- difference of the difference of *fut2CArcti* minus *present-day* (upper rows) and *fut2CArcti* minus *piArctic* (lower rows) ensemble means, near surface temperature (K) (at left) and pressure at sea level (hPa) (at right). Shading indicates significance at $p < 0.1$.

Drivers of High-Latitude Blocking activity

Atmospheric blocking is associated with weather extremes, which can instigate life threatening conditions with severe societal impacts. Here, we investigate the impact of local Arctic sea-ice and remote sea surface temperature on blocking activity over the Northern Hemisphere mid- and especially high-latitudes. We employ a modified version of the Absolute Geopotential Height (AGH) reversal blocking algorithm that is able to capture high-latitude blocking more adequately than previous versions (Tyrlis et al. 2021). The improved representation of high-latitude blocking will help disentangle the impact of remote and local drivers on the frequency of blocking occurrence and related extremes.

Winter blocking diagnosis produced by the MPI-ESM generally tends to underestimate blocking activity compared to ERA-INTERIM reanalysis (e.g., Müller et al. 2018). The salient features of mid-latitude Blocking Episode (BE) activity over the North Atlantic, Europe, Ural

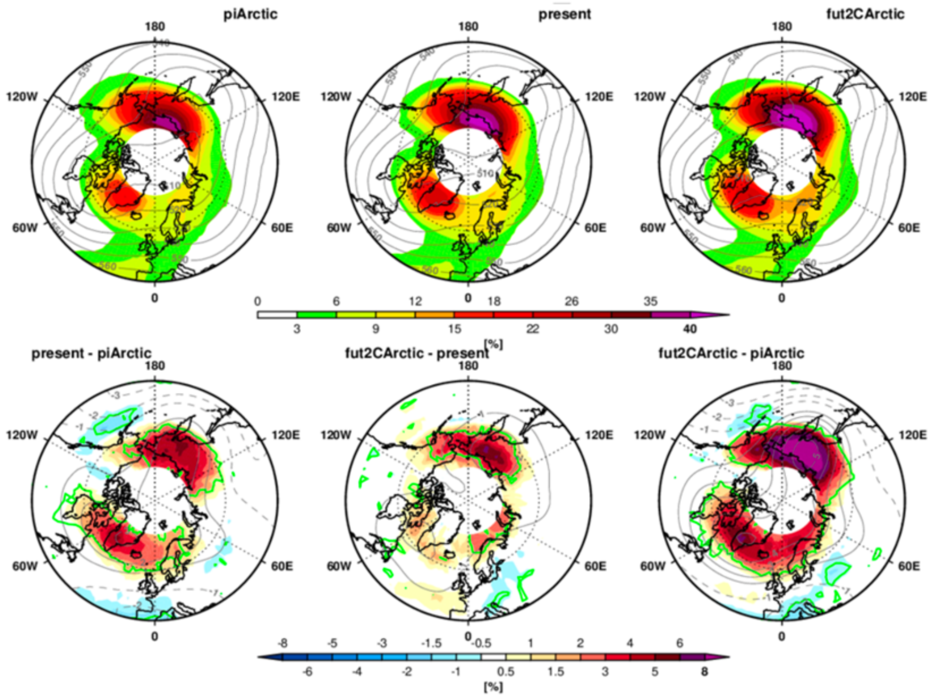

Mountain region and central-eastern North Pacific can be identified. The main activity of high-latitude blocking occurs mainly over Greenland and the Bering Straits (Figure 6, top row). Our first findings indicate that Arctic Sea Ice loss is connected to a robust increase in geopotential heights over the Arctic, especially over Greenland and Far East Asia, on the poleward side of the Atlantic and Pacific eddy-driven jets (Figure 6, bottom row). This is associated with increasing high-latitude blocking activity over these two regions.

Figure 6: Upper row: DJF BE frequency (shaded, %) and 500 hPa Geopotential Height (contours, dm) corresponding to *piArctic* (left), *present-day* (middle) and *fut2CArctic* (right) ensemble means. Bottom row: Difference of *present-day* minus *piArctic* (left), *fut2CArctic* minus *present-day* (middle) and *fut2CArctic* minus *piArctic* (right) ensemble-mean BE (shaded, %) and 500 hPa Geopotential Height (contours, dm). Green line encloses areas for which $p < 0.05$ and the blocking activity change can be considered as statistically significant at the 5% level.

Under all pre-industrial, present and future Arctic Sea Ice conditions, the oceanic state AMV-/IPV+ is associated with a deeper Aleutian Low and a stronger Ridge over North America compared to AMV+IPV- conditions. Thus, during the state AMV-/IPV+, more frequent blocking is observed over Alaska and the Bering Straits but less blocking further to the south (Figure 7, top row). This dependence of blocking activity over the region on the oceanic state appears to emerge stronger in *present-day* and *fut2CArctic* experimental set-ups rather than in *piArctic*. We found a weak dependence of the blocking activity on the phase of the QBO. There is a tendency for more frequent high-latitude blocking in QBOE but this signal varies under pre-industrial, present and future Arctic Sea Ice conditions (Figure 7, bottom row).

Stratification of the impact of Arctic Sea Ice decline on the blocking activity with respect to the oceanic state suggests that the increase in High-Latitude Blocking activity is higher under the regime AMV-/IPV+ rather than AMV+/IPV-. This is more evident for Greenland blocking (Figure 8). We report no strong dependence of the increase in high-latitude blocking activity following Sea Ice loss on the phase of the QBO.

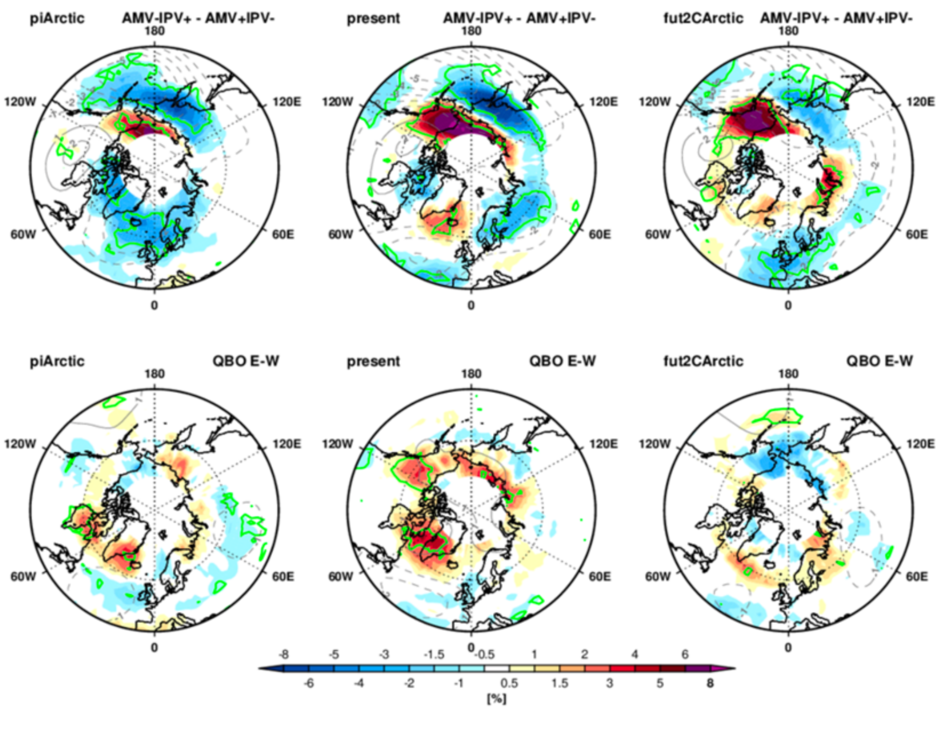

Figure 7: Upper row: Difference AMV-IPV+ minus AMV+IPV- for DJF BE frequency (shaded, %) and 500 hPa geopotential height (contours, dm) for *piArctic* (left), *present-day* (middle) and *fut2CArctic* (right) ensemble-means. Bottom row: Difference between QBO East minus QBO West for DJF BE frequency (shaded, %) and 500 hPa geopotential height (contours, dm) for *piArctic* (left), *present-day* (middle) and *fut2CArctic* (right) ensemble means. Green line encloses areas for which $p < 0.05$ and the blocking activity change can be considered as statistically significant at the 5% level.

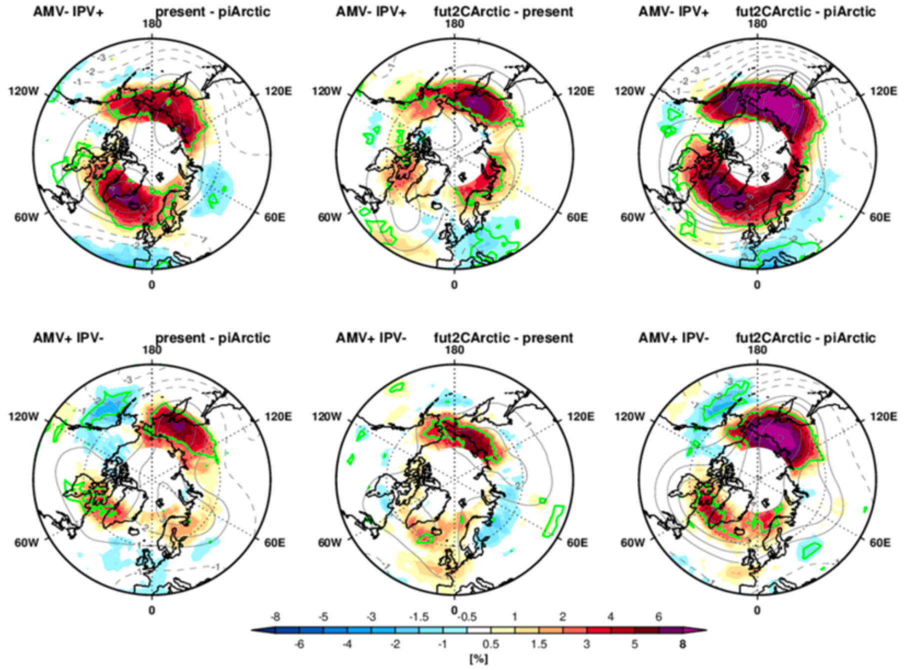

Figure 8: Upper row: Difference of *present-day* minus *piArctic* (left), *fut2CArctic* minus *present-day* (middle) and *fut2CArctic* minus *piArctic* (right) ensemble-mean BE frequency (shaded, %) and 500 hPa geopotential height (contours, dm) for ocean state AMV-IPV+. Bottom row: As upper row but AMV+IPV-. Green line encloses areas for which $p < 0.05$ and the blocking activity change can be considered as statistically significant at the 5% level.

References

Bunzel, F., D. Notz, J. Baehr, W.A. Müller, and K. Fröhlich (2016). Seasonal climate forecasts significantly affected by observational uncertainty of Arctic sea ice concentration. *Geophysical Research Letters*, 43, 852-859, doi:10.1002/2015GL066928.

Mauritsen, T., and Co-Authors (2019). Developments in the MPI-M Earth System Model version 1.2 (MPI-ESM1.2) and its response to increasing CO_2. *Journal of Advances in Modeling Earth Systems*, 11, 998-1038, doi:/10.1029/2018MS001400.

Müller, W. A., and Co-Authors (2018). A higher-resolution version of the Max Planck Institute Earth System Model (MPI-ESM1.2-HR). *Journal of Advances in Modeling Earth Systems*, 10, 1383–1413. https://doi.org/10.1029/2017MS001217

Smith, D., Screen, J., Deser, C., Cohen, J., Fyfe, J., Garcia-Serrano, J., Jung, T., Kattsov, V., Matei, D., Msadek, R., Peings, Y., Sigmond, M., Ukita, J., Yoon, J.-H. & Zhang, X. (2019). The Polar Amplification Model Intercomparison Project (PAMIP) contribution to CMIP6: investigating the causes and consequences of polar amplification. *Geoscientific Model Development*, *12*, 1139-1164.

Tyrlis, E., J. Bader, E. Manzini, and D. Matei, D (2021) Reconciling different methods for high-latitude blocking detection. *Quarterly Journal of the Royal Meteorological Society*, 147, 1070-1096. DOI: 10.1002/qj.3960.